Petroleum Science 20 (2023) 2187–2201

Contents lists available at ScienceDirect

Petroleum Science

journal homepage: www.keaipublishing.com/en/journals/petroleum-science

Original Paper

The enhancement of performance and imbibition effect of slickwater-based fracturing fluid by using MoS_2 nanosheets

Hang Xu [a, b], Yuan Li [a, b], Guo-Lin Yu [a, b], Sa-Sa Yang [a, b], Bo-Jun Li [a, b], Fu-Jian Zhou [a, b, *], Er-Dong Yao [a, b, **], Hao Bai [a, b], Zhi-Yu Liu [a, b]

[a] Unconventional Petroleum Research Institute, China University of Petroleum (Beijing), Beijing, 102249, China
[b] National Key Laboratory of Petroleum Resources and Engineering, China University of Petroleum (Beijing), Beijing, 102249, China

ARTICLE INFO

Article history:
Received 7 June 2022
Received in revised form
13 December 2022
Accepted 18 December 2022
Available online 20 December 2022

Edited by Yan-Hua Sun

Keywords:
Slickwater-based fracturing fluid
MoS_2 nanosheet
Performance evaluation spontaneous imbibition
Climbing film

ABSTRACT

Slickwater-based fracturing fluid has recently garnered significant attention as the major fluid for volumetric fracturing; however, lots of challenges and limitations such as low viscosity, poor salt tolerance, and possible formation damage hinder the application of the conventional simple slickwater-based fracturing fluid. In addition, nanomaterials have proven to be potential solutions or improvements to a number of challenges associated with the slickwater. In this paper, molybdenum disulfide (MoS_2) nanosheets were chemically synthesized by hydrothermal method and applied to improve the performance of conventional slickwater-based fracturing fluid. Firstly, the microstructure characteristics and crystal type of the MoS_2 nanosheets were analyzed by SEM, EDS, TEM, XPS, and Raman spectroscopy techniques. Then, a series of evaluation experiments were carried out to compare the performance of MoS_2 nanosheet-modified slickwater with the conventional slickwater, including rheology, drag reduction, and sand suspension. Finally, the enhanced imbibition capacity and potential mechanism of the nanosheet-modified slickwater were systematically investigated. The results showed that the self-synthesized MoS_2 nanosheets displayed a distinct ultrathin flake-like morphology and a lateral size in the range of tens of nanometers. In the nano-composites, each MoS_2 nanosheet plays the role of cross-linking point, so as to make the spatial structure of the entire system more compact. Moreover, nanosheet-modified slickwater demonstrates more excellent properties in rheology, drag reduction, and sand suspension. The nanosheet-modified slickwater has a higher apparent viscosity after shearing 120 min under 90 °C and 170 s^{-1}. The maximum drag reduction rate achieved 76.3% at 20 °C, and the sand settling time of proppants with different mesh in the nano-composites was prolonged. Spontaneous imbibition experiments showed that the gel-breaking fluid of nanosheet-modified slickwater exhibited excellent capability of oil-detaching, and increase the oil recovery to ~35.43%. By observing and analyzing the interfacial behavior of MoS_2 nanosheets under stimulated reservoir conditions, it was found that the presence of an interfacial tension gradient and the formation of a climbing film may play an essential role in the spontaneous imbibition mechanism. This work innovatively uses two-dimensional MoS_2 nanosheets to modify regular slickwater and confirms the feasibility of flake-like nanomaterials to improve the performance of slickwater. The study also reveals the underlying mechanism of enhanced imbibition efficiency of the nano-composites.

1. Introduction

Unconventional oil and gas, such as shale gas and tight oil, have become essential substitute resources in the 21st century (Li Y. et al., 2022a; Wei et al., 2021; Song et al., 2022). Due to the ultra-low permeability and porosity of the unconventional resources, large-scale volumetric fracturing is necessary to form the complex

* Corresponding author. Unconventional Petroleum Research Institute, China University of Petroleum (Beijing), Beijing, 102249, China.
** Corresponding author. Unconventional Petroleum Research Institute, China University of Petroleum (Beijing), Beijing, 102249, China.
E-mail addresses: zhoufj@cup.edu.cn (F.-J. Zhou), yaoed@cup.edu.cn (E.-D. Yao).

https://doi.org/10.1016/j.petsci.2022.12.008

fracture network system and expand the stimulated reservoir volume (Li M. et al., 2021, 2022; Wei et al., 2022). Recent studies suggested that after hydraulic fracking, the fracturing fluid creates a stimulated reservoir domain with higher porosity, higher permeability, and changed rock compressibility compared to the unstimulated reservoir to improve oil/gas production (Cui et al., 2020; Li W. et al., 2020, 2022; Li et al., 2022b). To meet the needs of large-scale volumetric fracturing, slickwater-based fracturing fluids are widely used because of their strong fracture formation ability and natural fracture communication ability. There are various additives in slickwater-based fracturing fluid, but drag reducer is the core component and its performance is closely related to fracturing operation parameters, and directly affects the creation of the stimulated reservoir.

In recent years, improving the performance of slickwater and developing functional fracturing fluids have become important research directions in volumetric fracturing in unconventional reservoirs. As the essential component in any slickwater-based fracturing fluids, the drag reducer has attracted special attention. There are many kinds of drag reducers reported in previous literature, but polyacrylamides are the most widely used water-soluble drag reducers in the stimulation process of unconventional reservoirs (Al-Sarkhi, 2010; Bai et al., 2021). Polyacrylamide (PAM) is a synthetic polymer obtained by copolymerizing acrylamide and other monomers, including cationic, anionic, nonionic, and amphoteric polyacrylamide (Barati and Liang, 2014; Chen et al., 2020; Kot et al., 2012). The presence of many amide groups in the main chain of polyacrylamide gives it high activity and controllable performance, which determines its intended use and specific physical behavior in aqueous media (Ismail et al., 2022). Related studies have shown that PAM polymer itself has a certain drag reduction effect. Regarding the drag reduction mechanism, the mainstream view is that the polymers can inhibit the formation of a turbulent vortex, and reduce the turbulent pulsation and flow resistance of the fluid. The conformation of polymer chains in the solution varies with flow rates, and the appearance of complex interactions between polymers and vortexes leads to the alteration of the flow field and turbulent structures, which results in a visible drag reduction effectiveness (Edomwonyi-Otu et al., 2015; Habibpour and Clark, 2017; Warholic et al., 1999). However, PAM usually presents unsatisfactory performance under harsh reservoir conditions such as in high temperature or high salinity reservoirs. Moreover, because of the mechanical scission of PAM polymer chains under high shear rates, it usually presents a poor drag reduction effectiveness.

Some researchers have shown that modification of the PAM with special hydrophobic monomers can improve the rheological properties and temperature or salt resistance of the slickwater (Kot et al., 2012). Ibrahim et al. (2018) obtained a PAM-acrylic acid copolymer drag reducer by modifying PAM with hydrophobic monomer Z. Performance evaluation results show that the drag reduction of the new drag reducer was higher than 70% in freshwater or with 2 wt% potassium chloride in the presence of calcium chloride. Modification of PAM with monomers containing sulfonic acid groups, such as vinyl sulfonic acid, propylene sulfonic acid, 2-acrylamide-2-methyl propane sulfonic acid (AMPS), can not only increase the water solubility of the copolymer but also improve the temperature and salt resistance of the copolymer. Except for chemical modification, the addition of surfactants or other additives as a booster to regular drag reducers can also provide some improvement towards a certain performance. Seymour et al. (2018) studied the synergistic effect of surfactant and partially hydrolyzed PAM to enhance the salt tolerance of drag reducer, and there is a significant reduction in inversion time and increase in maximum drag reduction in all tested high-salinity brines when the surfactant is added with the drag reducer. These solutions often result in an improvement in the single performance of the slickwater, but it is difficult to significantly strengthen the performance of slickwater. Meanwhile, these modifications often increase the cost of the drag reducer (Shen et al., 2019).

Nanotechnology is a popular method to effectively improve the performance of fracturing fluid. Nanomaterials have unique physicochemical properties, such as size effect, strong adsorption force, and surface modifiability, which can penetrate deep into the reservoir without the restriction of pore throat size (Al-Muntasheri et al., 2017; Lafitte et al., 2012; Yekeen et al., 2019). It was found that the addition of nanomaterials to water-based fracturing fluid can reduce the flow friction of the fracturing fluid, improve the sand-carrying performance, lower the surface and interfacial tension, and enhance the oil displacement effect. Nanomaterials have played a pivotal role in improving fracturing fluids composed of polymers, especially in drag reduction (Yekeen et al., 2019). Yu et al. (2015) successfully developed a slickwater system using nanomaterials, which was favored by its low damage to the reservoir, strong temperature and salinity resistance, and high drag reduction rate of up to 75%. Xing et al. (2019) synthesized nanocomposites with exfoliated montmorillonite sheets via in situ free radical copolymerization, and the drag reduction performance of nanocomposites improved up to 58% in the high *Re* region at a concentration of 300 ppm. Li X. et al. (2022) explored the underlying mechanism of the nanoparticle-induced drag reduction for PAM in turbulent flow with high Reynolds numbers. They found that the addition of SiO_2 nanoparticles to cationic PAM solution was quite efficient for reducing drag only at Reynolds numbers more than 6000. At present, most studies about the application of nanomaterials in fracturing fluids still focus on nano-composite formula optimization and performance evaluation; there still needs more comprehensive studies on the synergistic effects and the interaction between various nanomaterials and polymer-based frac fluid (Krishnan et al., 2016; Li et al., 2019).

Nowadays, the potential of nanoparticles to enhance oil recovery in free imbibition tests or core-flooding tests has also attracted much attention in the literature. Rostami et al. (2019) used salt-containing silica nanofluid to improve oil recovery. The results show that silica nanoparticles can alter the wettability of glass and sandstone surfaces to more water-wet conditions. Due to the more adsorption of nanoparticles on the rock surface, the presence of salt in nanofluids also shows a significant positive effect on the wettability alteration level. Qing et al. (2022) investigated the effect of self-synthesized α-zirconium phosphate (α-ZrP) nanosheets on the reduction of oil-water interfacial tension and wettability alteration. The results of coreflooding experiments show that the oil recovery efficiency increased from 33.59% to 51.26% when α-ZrP nanosheets concentrations increased from 50 to 1000 ppm. Nikolov et al. (2010) used combined differential and ordinary light interferometry to study the solid-nanofluid-oil interaction for the first time and directly observed the self-structuring features of nanoparticles. The ordering of these microstructures in the wedge region leads to excessive pressure in the film relative to the bulk solution (i.e., the structural disjoining pressure), thus separating the two surfaces confining the nanofluids. Keykhosravi et al. (2021) proposed an ideal solution for SiO_2 nanoparticles to achieve the highest recovery. It was reported that while nanoparticles can rapidly reduce interfacial tension, they require at least 7 days to alter the carbonate surface's wettability optimally. Nanoparticles soaked in core samples for a week recovered about 80 percent of the original oil in place.

Nonetheless, there have been few studies on nano-composites slickwater-based fracturing fluids formed by PAM polymer and nanomaterials. Additionally, no scholar has paid attention to the

effect of two-dimensional nanomaterials on the properties of slickwater-based fracturing fluids and the enhanced imbibition mechanism. Herein, this paper would like to determine whether MoS_2 nanosheet can improve the performance of the conventional slickwater-based fracturing fluid, including rheology, drag reduction, sand suspension, and spontaneous imbibition. Furthermore, the synergistic mechanism between MoS_2 nanosheet and slickwater-based fracturing fluid was revealed, and the potential mechanism of two-dimensional nanosheet enhanced imbibition was explained through an interfacial behavior experiment.

2. Materials and methods

2.1. Materials

In this work, a highly viscous drag reducer (DR-900) was used, which was provided by Beijing Kemax Oilfield Chemicals Company, China. DR-900 is a cationic polyacrylamide copolymer with a molecular weight of 8×10^6, white emulsion, avirulent and insipidity. Chemical grade sodium molybdate, citric acid, thioacetamide, and ethanol employed to prepare MoS_2 nanosheets were purchased from Aladdin Biochemical Technology Co., Ltd (Shanghai, China). Ammonium persulfate with analytical purity was used as a gel-breaker, was purchased from China State Pharmaceutical Group Chemical Reagent Co., Ltd. (Beijing, China). Sodium chloride, magnesium chloride, and calcium chloride, of analytical purity, were provided by Hongyan Chemical Reagent Factory (Tianjin, China).

The core samples were obtained from the tight oil block of Changqing Oilfield where the oil-bearing is in the range of 2562–2596 m. Both porosity and permeability of the core samples were measured by nitrogen with high purity. The permeabilities and porosities of these dried cores were in the ranges of 0.045–0.092 mD and 8.24%–13.47%, respectively. Table 1 presents the basic parameters of the core samples, in which the C2 and C3 cores with similar properties were used to carry out the subsequent imbibition experiments. The experimental oil used in this study is stock tank oil, which was taken from the Changqing Oilfield as well. At the temperature of 80 °C and atmospheric pressure, the oil viscosity is 1.45 mPa s, and the density is 0.864 g/cm^3.

2.2. Methods

2.2.1. MoS_2 nanosheet preparation

The preparation of MoS_2 nanosheets includes physical and chemical synthesis methods. The physical method mainly includes mechanical grinding and ultrasonic peeling, while the chemical method is more flexible, such as the hydrothermal method, microemulsion synthesis method, chemical deposition method, etc. (Zhang, 2015). In this study, the MoS_2 nanomaterial was synthesized by the hydrothermal method. Sodium molybdate, citric acid and thioacetamide were mixed in 100 mL of deionized water with the mass of 0.1, 0.1, and 1 g, respectively. The well-stirred solution was transferred to a 150-mL autoclave and heated at 200 °C for 10 h. Afterward, the precipitated nanosheets were first washed with deionized water three times (approximately 0.2–0.3 g nanosheets per 500 mL) and then washed with ethanol three times (approximately 0.2–0.3 g nanosheets per 100 mL). After washing, the nanosheets were centrifuged at 5000 rpm for 30 min to obtain MoS_2 nanosheets. The following chemical reactions can represent the whole reaction process. First, the hydrolysis of ammonium thioacetate produces hydrogen sulfide gas, which acts as both a sulfur source and a reducing agent, reducing Mo(VI) to Mo(IV), and finally forming MoS_2 nanosheets.

$$CH_3CSNH_2 + H_2O \rightarrow CH_3CONH_2 + H_2S$$

$$4MoO_4^{2-} + 6CH_3CONH_2 + 9H_2S \rightarrow 4MoS_2 + 6CH_3COO^- + SO_4^{2-} + 6H_2O + 6NH_3\uparrow$$

Table 1
The basic parameters of the core samples.

Sample No.	Length, mm	Diameter, mm	Permeability, mD	Porosity, %
C1	5.134	2.503	0.045	8.24
C2	5.116	2.512	0.063	11.09
C3	5.089	2.508	0.069	10.76
C4	5.067	2.506	0.084	13.47
C5	5.124	2.510	0.092	12.39

2.2.2. Preparation of MoS_2 nanosheet-modified slickwater

Previous studies have shown that nanomaterial has a direct improvement effect on the performance of slickwater-based fracturing fluid. Still, there is often a critical value that can ensure the best improvement effect (Al-Muntasheri et al., 2017; Lafitte et al., 2012). According to the amounts of various additives used in the oilfield, the dosage range of drag reducer is usually 0.05–1.0 wt%, the concentration of nanomaterials is 0.01–0.1 wt% (Liu et al., 2020). The low-viscosity slickwater-based fracturing fluid is mainly used as the pad fluid to create fractures, while the sand-carrying fluid stage requires a higher viscosity slickwater system, usually by increasing the concentration of drag reducer to improve the viscosity. Based on the existing research, to meet the experimental requirements of the subsequent static sand suspension tests, the preferred amount of DR-900 in this study is 0.5% (Liu et al., 2022). On this basis, the DR-900 slickwater-based fracturing fluid will further be nanosheet-modified and the amount of MoS_2 was optimized to obtain the best formulation. It's worth noting that other additives have relatively small contents and high compatibility, such as bactericide, deoxidant and clay stabilizer, which will not affect the performance of the nano-modified fracturing fluid.

2.2.3. Instrumental characterizations

The morphologies of self-synthesized MoS_2 nanosheets were characterized by environmental scanning electron microscope (E-SEM, Quanta 200, FEI, Netherlands) and transmission electron microscopy (TEM, JEM-2100F, Hitachi, Japan), respectively. The element distribution scanning (EDS) of the MoS_2 nanosheets was obtained by scanning transmission electron microscopy equipped with high angular annular dark field detector. The crystal structure of MoS_2 nanosheets was identified by Raman spectroscopy (LabRAM HR800, Horiba, France), and the wavelength of the excitation light source used is 532 nm (50 mW), the spot size is about 1 μm, and the wavelength band of 100–500 cm^{-1} is mainly selected for analysis. The chemical composition of MoS_2 nanosheets was analyzed using an X-ray photoelectron spectrometer (XPS, Nexsa G2, Thermo Fisher Scientific, USA) with Al Kα X-rays as the excitation source. The thermal properties of both DR-900 slickwater and MoS_2 nanosheet-modified DR-900 slickwater fracturing fluid were recorded by thermogravimetric analysis (TGA, DSC 7020, Hitachi, Japan) in nitrogen atmosphere from ambient temperature to 800 °C with a heating rate of 20 °C/min.

2.2.4. Rheological property test

Among the numerous properties of fracturing fluids that affect the field operation, the most important is rheology. It involves the design of the most significant parameters such as stability, suspension capacity, and drag calculation of the injected fluid during

the fracturing process. This paper mainly focuses on the apparent viscosity and viscoelastic modulus of the DR-900 and MoS_2 nanosheet-modified DR-900 slickwater-based fracturing fluid. Apparent viscosity can reflect the temperature and shear resistance of slickwater, which is related to the stability of fracturing fluid. Viscoelastic modulus reflects the viscoelastic characteristics of slickwater, which is related to the sand suspension performance of fracturing fluid.

The conventional DR-900 slickwater and the optimal MoS_2 nanosheet-modified DR-900 slickwater systems were separately loaded into a HAAKE MARS III rheometer to conduct temperature and shear resistance tests. Ramping up to 90 °C at a rate of 4.5±0.5 °C/min, and shear it for 120 min under 170 s^{-1}. 170.3 s^{-1} usually represents the wellbore shear rate in the field (Bai et al., 2021). The apparent viscosity varying with time was recorded to evaluate the shear resistance, and the final retained apparent viscosity after shearing reflected the thermal and shear stability of slickwater-based fracturing fluids.

Viscoelasticity is one of the main indexes reflecting the sand suspension performance of polymer fluid. There is a recognized fact that the lower the crossover value of the viscous modulus G'' and the elastic modulus G', the greater the sand-carrying capacity of the corresponding fluid. The viscoelasticity of DR-900 slickwater and nanosheet-modified DR-900 slickwater were tested using the HAAKE RS6000 rheometer to shear them from low-to-high frequency under some tension. Firstly, stress sweeping of the slickwater system was carried out, and then the stress values near the inflection point were scanned by the frequency method to obtain the elastic modulus and the viscous models of the tested fluid. According to the crossover point value, the viscoelastic strength of the two kinds of slickwater was determined.

The salt resistance test is to study the effect of metal ions in the formation water on the apparent viscosity of slickwater. The type and concentration of ions measured in this study refer to the actual water quality condition in the oilfield. This study tested the effect of three different metal ions: Na^+, Mg^{2+}, and Ca^{2+} at different concentrations on the apparent viscosity of DR-900 slickwater and nanosheet-modified DR-900 slickwater at room temperature. The salinity of the three mental ions was selected as 500, 1000, 1500, and 2000 ppm. Taking 500 ppm sodium chloride solution as an example, it can be obtained by weighing 0.05 g solid sodium chloride and dissolving it in 99.95 g deionized water. After fully stirring and completely dissolving in deionized water, an appropriate amount of drag reducer and MoS_2 nanosheets were added to the brine to prepare the nanosheet-modified slickwater-based fracturing fluid. At last, a six-speed rotational viscometer was used to test the apparent viscosity of the slickwater-based fracturing fluid under different salinity conditions.

2.2.5. Drag reduction test

Compared with the conventional guar gum biopolymer fracturing fluid, the slickwater-based fracturing fluid has lower wellbore flow drag, which reduces the drag pressure drop flowing in the wellbore and avoids the problem of excessive wellhead pressure (Xu et al., 2022; Yao et al., 2021). Therefore, the drag reduction performance evaluation of DR-900 slickwater and nanosheet-modified DR-900 slickwater was carried out in this study.

The drag pressure was measured by the difference generated when freshwater and slickwater-based fracturing fluid flowed through the same straight pipe, respectively, and the drag reduction rate can be calculated by Eq. (1). The YMC-2 type loop drag test system, which mainly consists of a screw pump, a liquid supply system, a pipeline system, and a integrated control computer, was employed to test the drag reduction rate in this study. Details about the self-developed device and usage procedures can be found in the published literature (Bai et al., 2021). During the experiment, the displacement of the screw pump gradually increased from 250 to 2500 kg/h, and the interval is 250 kg/h. Thus, the corresponding relationship between the drag reduction rate and the displacement could be obtained.

$$R_{DR} = \frac{\Delta P_w - \Delta P_s}{\Delta P_w} \times 100\% \quad (1)$$

where R_{DR} is the drag reduction rate, %; ΔP_w is the drag pressure difference generated by freshwater, MPa; ΔP_s is the drag pressure difference generated by slickwater-based fracturing fluid, MPa.

2.2.6. Sand suspension performance test

Sand suspension is the most basic index of proppant optimization, and one of the key factors in determining the success or failure of fracturing stimulation operation. At present, there are two methods for testing and evaluating the sand suspension and proppant settling performance of fracturing fluid in the laboratory: one is the single-particle proppant settling method based on the Stokes theory formula, and the other is the sand-carrying fluid (multi-particle) suspension performance test method (Ba Geri et al., 2019; Biheri and Imqam, 2022). The multi-particle experimental method more objectively reflects the sand suspension and proppant settling characteristics of fracturing fluid and is closer to the actual fracturing situation.

In this study, the static sand suspension properties of two slickwater systems (DR-900 and nanosheet-modified DR-900) were tested separately. All the slickwater fluids were prepared and mixed with deionized water. The static settling experiments used four proppant sizes (i.e., 20/40, 40/60, 60/80, and 80/100 mesh). Specified graduated cylinders were used in this experiment to measure sand fall rate in unconfined fractures. Stir well in the beaker to mix the proppant in the slickwater-based fracturing fluid evenly, then pour the sand-carrying fluid into the graduated glass cylinder, and record the time when the suspended proppant settles to the bottom of the graduated cylinder. According to the initial suspension column height and settling time, the settling velocity of proppants with different mesh in the slickwater-based fracturing fluid system can be calculated.

2.2.7. Spontaneous imbibition effect test

Massive volumetric fracturing fluid is often used to create several man-made fractures in the actual fracturing process. While the flowback rate of the injected fracturing fluid is generally lower than 30% after stimulation, indicating that most of the fluid remains in the formation and is absorbed by the formation (Cao et al., 2022). During the operation of slickwater-based fracturing fluid, imbibition is the main method for reservoirs to absorb slickwater, and it is also an important driving force for improving oil well productivity (Li J. et al., 2022a, 2022b). The gel-breaking liquid of slickwater-based fracturing fluid in artificial fractures will enter the matrix through imbibition during the flowback process, displacing the residual oil in the micro-pores into the fractures, then the oil can flow along with the fracture network to the bottom hole (Bennion, 2002; Cheng, 2012; Liu et al., 2021).

Imbibition fluid. To meet the sand-carrying requirements, slickwater-based fracturing fluid often possesses a certain viscosity, but high-viscosity fluid is unable to enter the matrix pores by imbibition effect to displace residual oil. The so-called imbibition of fracturing fluid essentially refers to the process of the gel-breaking fluid into the matrix through dynamic/static imbibition during the soaking stage. The viscosity of the slickwater gel-breaking liquid is close to that of water, and it is easy to spontaneously imbibe into the micro-pores and throats to facilitate the interflow in the matrix

and replace more oil into the flow channels. In this study, ammonium persulfate was used as the gel breaker to break the DR-900 and nanosheet-modified DR-900 slickwater-based fracturing fluid systems at 80 °C in a water bath. The apparent viscosity of gel-breaking liquid was measured using capillary viscosity under reservoir temperature. When the viscosity of the gel-breaking fluid is lower than 5 mPa s, it is deemed completely broken. Then the gel-breaking liquid was poured into a Buchner funnel for vacuum filtration treatment to remove solid residues, and the filtrate in the suction flask was collected for subsequent imbibition experiments.

Experiment of oil drainage by imbibition. The slickwater gel-breaking liquid imbibition experiment adopts the volume method, and the experimental device is the Amott imbibition bottle. Before the test, a series of pretreatments were conducted to deal with the natural outcrop cores, including cutting, oil-washing, drying, weighing, and measuring some basic physical properties. Afterward, the treated cores were vacuumed for 48 h in a vessel and then saturated with the stock tank oil under a pressure of 15 MPa. Oil-saturated cores are aged for one week and then used to conduct imbibition tests. The formal imbibition experiment began with the prepared cores being completely immersed in the imbibition bottle filled with gel-breaking liquid, and the wetting phase fluid displaced the non-wetting phase fluid under the imbibition action. The Amott imbibition bottle was placed into an oven at 80 °C to simulate the actual reservoir temperature. The change of the concave liquid level in the pipe before and after imbibition indicates the amount of oil imbibed from the oil-saturated core, and then the imbibition recovery of the rock sample can be obtained. By recording the amount of oil produced at different times, the curve of imbibition recovery with time can be obtained. Fig. 1 illustrates the entire flow of the spontaneous imbibition experiment.

3. Results and discussion

3.1. Optimization of the dosage of MoS_2 nanosheet

As mentioned in Section 2.1.3, the viscosity of slickwater is often boosted by increasing the drag reducer concentration to meet the requirements of sand-carrying fluid in the field. In this study, the optimal concentration of DR-900 drag reducer is 0.5 wt%, according to the actual application status and suspended sand performance requirements (Liu et al., 2022). On this basis, the addition of MoS_2 was further optimized. A combination of ultrasonic treatment and mechanical stirring was used to disperse molybdenum disulfide nanosheets into DR-900 slickwater-based fracturing fluid to form nanosheet-modified systems with different concentrations. The apparent viscosity of the modified slickwater-based fracturing fluid system under different MoS_2 dosages at room temperature was tested using a six-speed rotary viscometer, and the experimental results are shown in Fig. 2. It can be seen from Fig. 2 that with the increase in shear rate, the apparent viscosity of different slickwater systems decreases significantly. A shear-thinning behavior was observed for all the slickwater systems because of the decrease in the viscosity at high shear rates. The comparison shows that the addition of nanomaterials can obviously improve the apparent viscosity of DR-900 slickwater, but it is not that the higher the

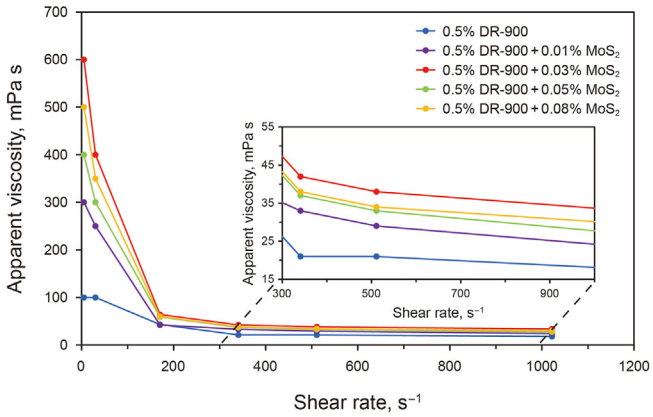

Fig. 2. Apparent viscosity of slickwater with different amounts of MoS_2 nanosheets.

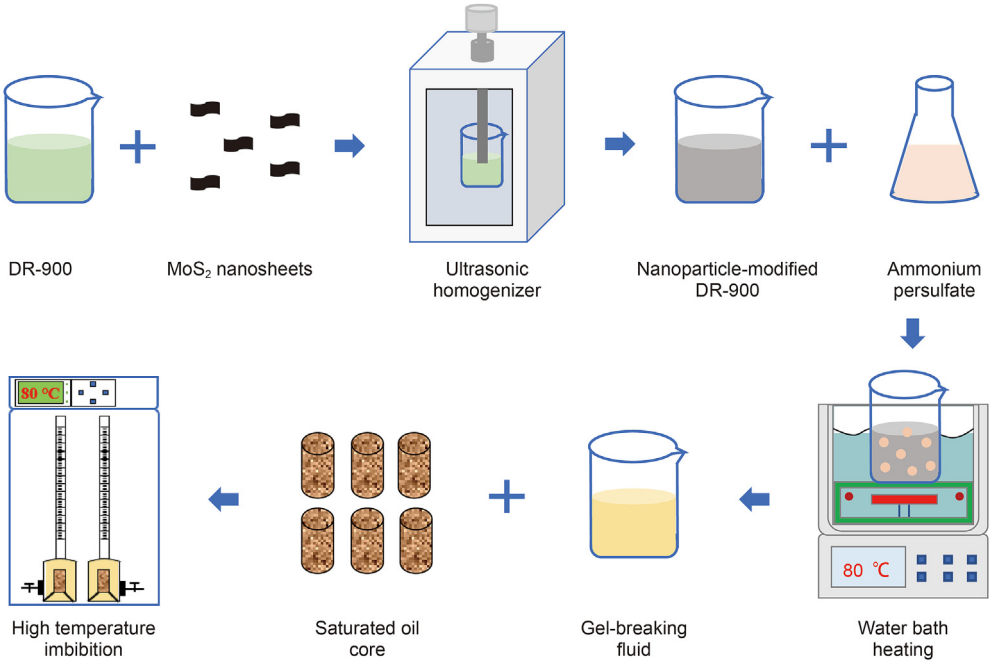

Fig. 1. Flow chart of spontaneous imbibition experiment.

amount of MoS_2 added, the greater the apparent viscosity of the modified system. The apparent viscosity value increased initially and decreased afterward. When the concentration of MoS_2 was 0.03 wt%, the apparent viscosity of the modified DR-900 slickwater was relatively high at various shear rates. However, with the further increase of MoS_2, the apparent viscosity decreases at various shear rates. These results indicate that there is an optimal value of MoS_2 addition, not that the more dosage, the better performance of the modified DR-900 slickwater. Analyzing the reasons, a high load of nanomaterial usually generates an over-crosslinking phenomenon, which made the nano-composite brittle and leads to a decrease in the viscosity of the modified DR-900 slickwater. This is mainly because of the nano effect, which causes a small amount of the MoS_2 nanosheets to aggregate into agglomerates and leads to poor dispersion of MoS_2 nanosheets (Liu et al., 2020). Then, the shear stability of the modified FR-900 structure formed is negatively affected.

3.2. Characterization

3.2.1. MoS_2 nanosheet

SEM and TEM. The morphology of the MoS_2 nanosheets synthesized by the hydrothermal method was observed by SEM, as shown in Fig. 3a. It can be seen from the magnified SEM image that the product is a relatively regular three-dimensional cluster-like structure and consists of many accumulated nanosheets, with a size of 20–40 nm. TEM images at different resolutions are also exhibited in Fig. 3b. The wide-field TEM images of 1T-MoS_2 show the edge of 2D layered nanosheets. The nanosheets in the 2D MoS_2 are stacked densely, and the number of stacked layers is between 3 and 5, with an interlayer separation of 0.63–0.65 nm. A small portion of the nanosheets was also slightly bent, similar to the phenomenon reported by Savjani et al. (2016). The reason for this is that such ultrathin nanosheets are unstable and easily form closed structures by rolling up to eliminate the dangling bonds at the edges (Zhang et al., 2016). EDS analysis was used to evaluate the weight percentage of MoS_2 elements. According to the results (Fig. 3c), the weight percentages of Mo and S were 34.73% and 65.27%, respectively.

Raman spectroscopy. The experimental results of Raman spectroscopy of the self-synthesized MoS_2 nanosheets are shown in Fig. 4. The strong Raman characteristic peak at 146 cm^{-1} is usually considered to be generated by stretching vibration between Mo–Mo bonds in MoS_2 of 1T crystal type, which is a typical Raman

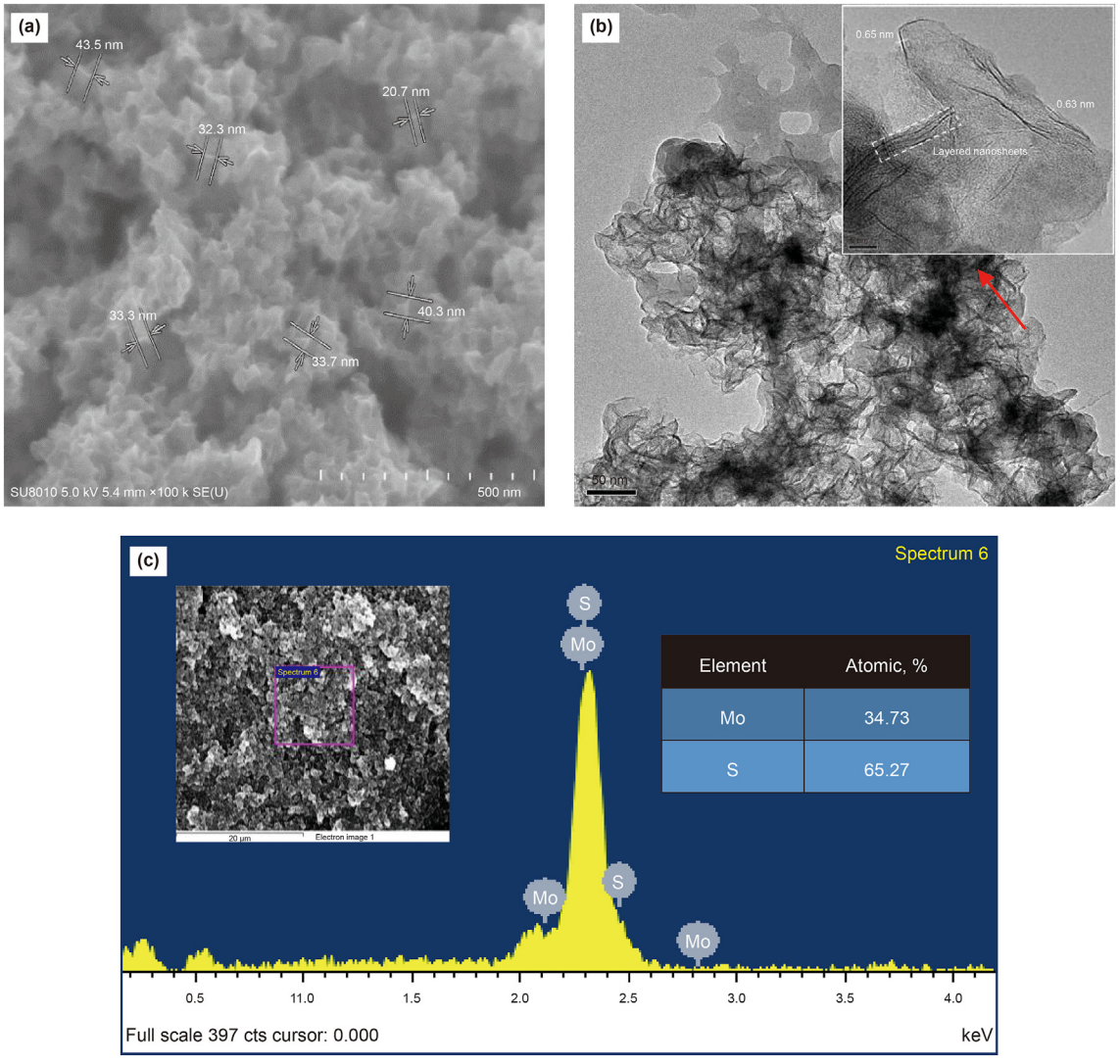

Fig. 3. SEM (**a**), TEM and high-resolution TEM (**b**), and EDS (**c**) of MoS_2 nanosheet.

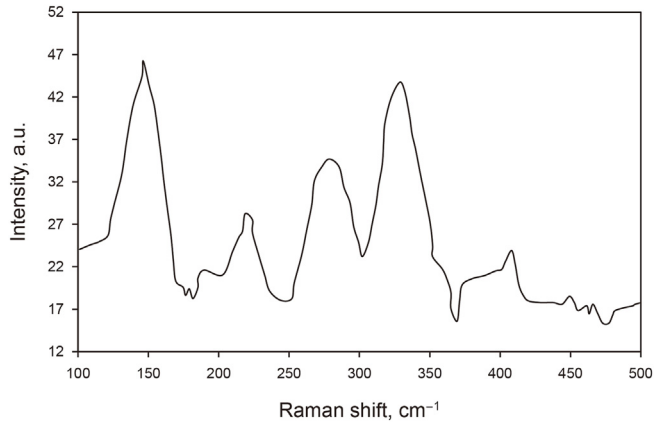

Fig. 4. Raman spectroscopy of MoS_2 nanosheet.

characteristic peak different from that of 2H crystal type. At the same time, obvious characteristic peaks are also observed at 220 and 324 cm^{-1}, which are related to the interface phonon mode of 1T crystal MoS_2. The peak at 409 cm^{-1} belonged to A^1_{2g}, corresponding to the relative vibration of the Mo–S bond along the direction perpendicular to the interlayer. The peak at 283 cm^{-1} belonged to A_{1g}, corresponding to the relative vibration mode of the Mo–S bond along the interlayer direction, indicating that the synthesized MoS_2 nanosheet has an octahedral structure. According to the results of Raman spectroscopic analysis, it can be determined that the synthesized product is MoS_2 with 1T crystal type.

XPS. The chemical composition of the synthesized MoS_2 nanosheet was further analyzed using X-ray photoelectron spectroscopy and the results are shown in Fig. 5. In the full spectrum (Fig. 5a), the range of 100–500 eV is selected for analysis, which includes the binding energy information of S 2*p*, Mo 3*d*, C 1*s* and Mo 3*p*. The presence of C 1*s* may be due to the incomplete reaction of part of the reducing agent. In Fig. 5b, the S 2*p* peaks of MoS_2 nanosheet were located at approximately 159.8 and 161.6 eV, and associated with S $2p_{3/2}$ and $2p_{1/2}$, respectively. Similarly, in Fig. 5c, the Mo 3*d* spectra consist of peaks located at approximately 226.8 and 230.1 eV, which correspond to the $3d_{5/2}$ and $3d_{3/2}$ components, respectively, of Mo^{4+} in the self-synthesized MoS_2 (Geng et al., 2016). The results of XPS spectra also confirmed that the synthesized MoS_2 nanosheets had a 1T crystal structure, which was consistent with the results of Raman spectroscopy.

3.2.2. Nanosheet-modified DR-900 slickwater

TGA. TGA was employed to acquire more information about the interaction between the DR-900 drag reducer and MoS_2 nanosheet. As shown in Fig. 6, the red and green lines represent the thermogravimetric (TG) curves of DR-900 slickwater and MoS_2 nanosheet-modified DR-900 slickwater, respectively, that is, the change of sample weight with temperature. The yellow line and the blue line represent the derivative thermogravimetric (DTG) curves of DR-900 slickwater and nanosheet-modified DR-900 slickwater, respectively, which are the results of a derivative of the TG curve, indicating the weight loss rate of sample changing with temperature, and its peak value is the maximum rate of sample weight decreases. Comparing the TG curves, the two samples have the almost same process of weight loss, but the ultimate weight loss of the DR-900 slickwater sample is 66.62%, and the nanosheet-modified DR-900 slickwater sample is 53.33%. This is because the polyacrylamide polymer and MoS_2 form a chemical bond, resulting in some components not being completely degraded at high temperatures, which is reflected in the increase of the residual weight

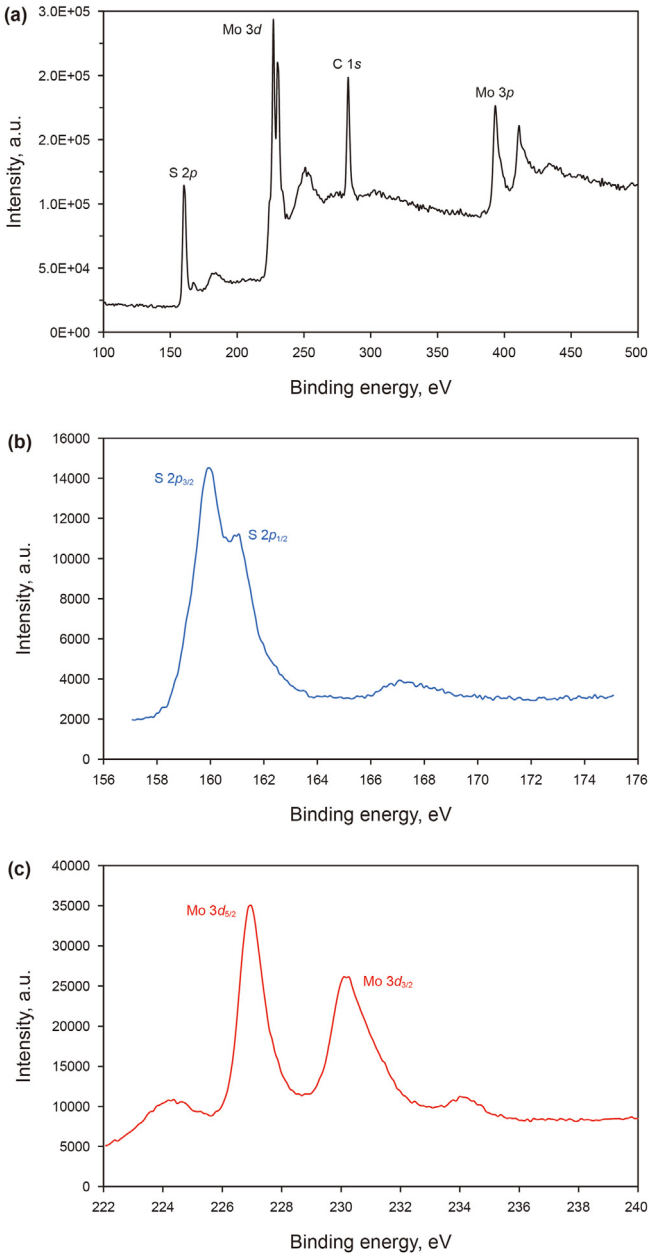

Fig. 5. High-resolution XPS full spectrum (**a**) and spectra of S 2*p* (**b**), Mo 3*d* (**c**) for MoS_2.

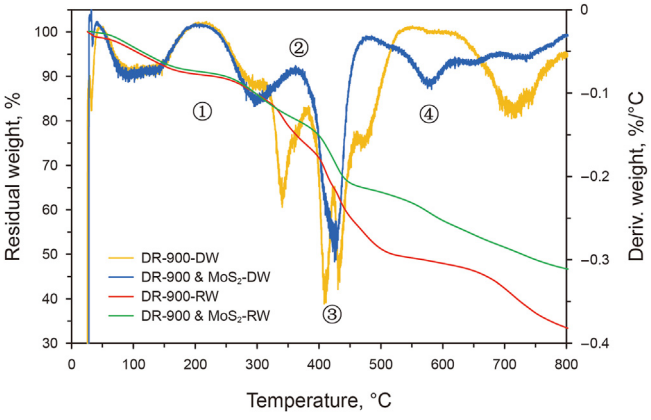

Fig. 6. The thermal gravimetric curves of two types of slickwater.

percentage compared with the conventional DR-900 system. It should be noted that the weight difference is not caused by the addition of MoS_2 since the concentration of MoS_2 nanosheets added is only 50 ppm.

Comparing the DTG curves, the two curves almost overlap in the first stage, indicating that the release process of the bound water adsorbed physically in the samples is basically the same. The second stage is the decomposition process of the amide bond inside the sample, and the decomposition rate of the DR-900 sample is significantly higher than that of the nanosheet-modified DR-900 sample. For the conventional DR-900 system, the amide bond in the polyacrylamide molecule will decompose directly at about 340 °C, while the MoS_2 and the amide bond have a binding force, resulting in an increase in the decomposition temperature. The third stage is the decomposition process of the carbon skeleton. The conventional DR-900 system shows a multi-peak shape because it contains many kinds of monomers, while in the nanosheet-modified DR-900 system, the MoS_2 nanosheet forms a chemical bond with polyacrylamide, which changes the decomposition temperature and shows a single-peak shape. The fourth stage is the combustion stage of by-products and impurities after decomposition. TGA proved that every MoS_2 nanosheet in the modified DR-900 system acts as a node and plays an advantageous role in enhancing the properties.

SEM. Fig. 7 shows the SEM images of the conventional DR-900 slickwater and the nanosheet-modified DR-900 slickwater at different resolutions. The three-dimensional network structure features of polyacrylamide in DR-900 slickwater can be clearly seen in Fig. 7a and b, and its molecular shap exhibits circular features with an average size of 50–60 μm. Fig. 7c and d shows the microstructures of the nanosheet-modified DR-900 slickwater system. In comparison, the microstructure of the nanosheet-modified DR-900 slickwater system is much denser, with an average mesh size of only 5–10 μm, which is significantly smaller than that of the unmodified system at the same resolution. The bright white spot in the image is the MoS_2 nanosheets, which plays the nuclear crosslinking point and skeleton role in the complex network structure. After compounding MoS_2 nanosheets, the mesh size of the network molecules in the slickwater became smaller, the network density increased, and the number of polymer aggregates in the solution increased.

A schematic diagram of crosslinking mechanism is shown in Fig. 8. In the nano-composite system, MoS_2 nanosheets are mostly clustered and adsorbed near the mesh node, and the suspended bonds or hole electrons on MoS_2 form covalent bonds with the hydroxyl groups on the polymer surface, creating a cross-linked structure inside the molecule. The aggregation of polymer

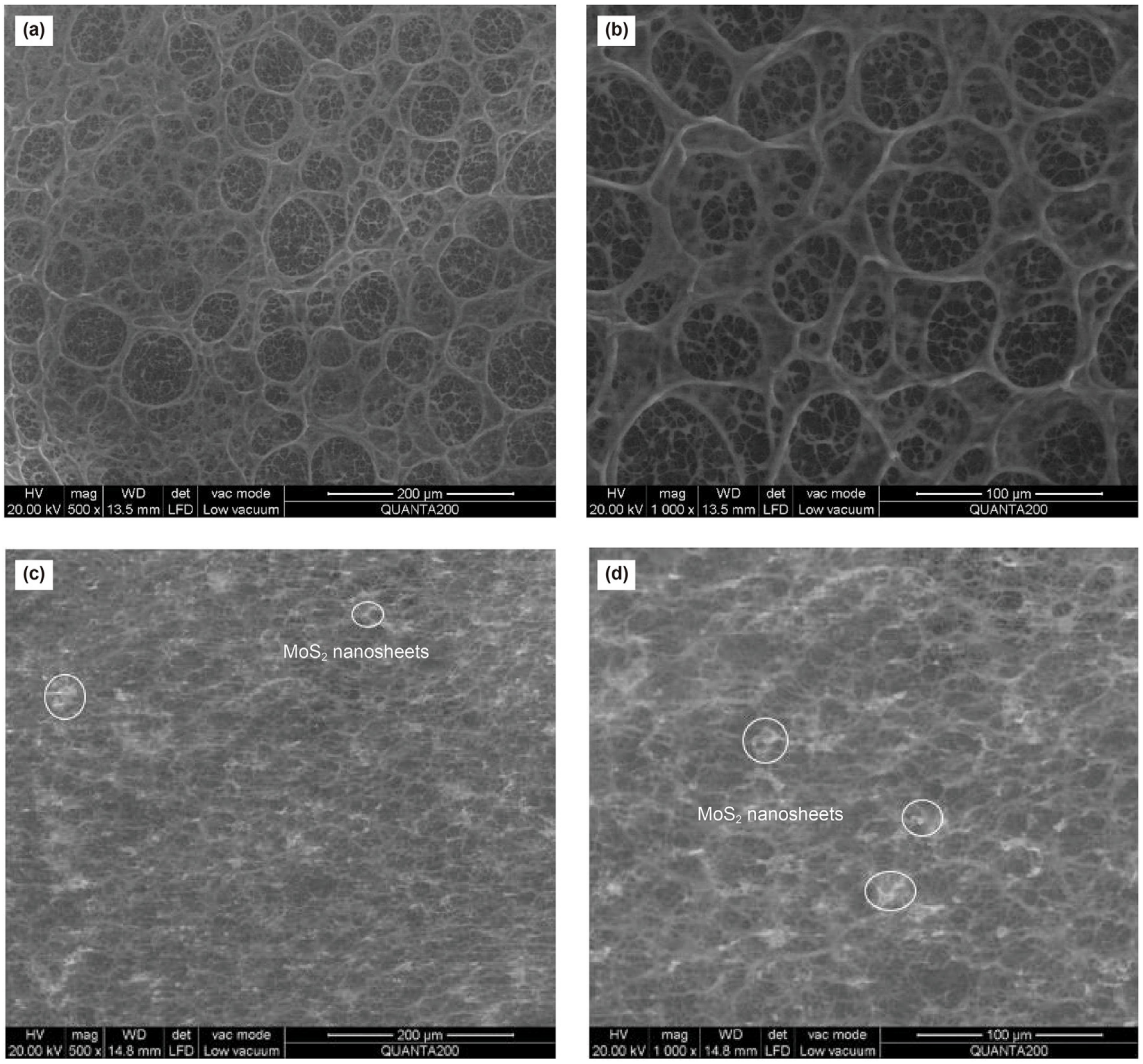

Fig. 7. SEM images of the conventional DR-900 slickwater (**a, b**) and the nanosheet-modified DR-900 slickwater (**c, d**) at different resolutions.

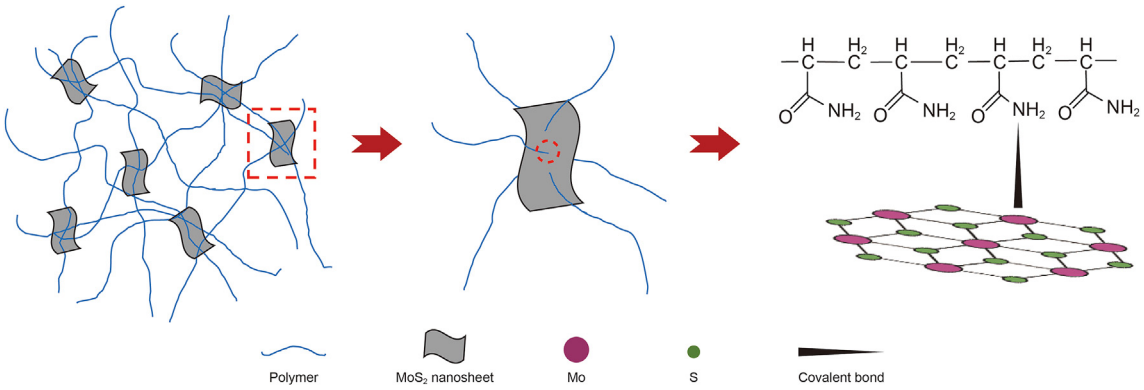

Fig. 8. Schematic diagram of MoS_2 nanosheets crosslinking with polymer.

molecules changes the original regular layered distribution, which makes the layers become disordered and the prototype of a spatial structure appears, thus enhancing the strength of the composite. At the same time, the addition of nanomaterials increases the contact area and molecular friction between layers. The MoS_2 "nodes" between the chains can protect the polymer molecules from shear fracture and maintain preferable strength, so the rheological and viscoelastic properties of the nano-composites were enhanced. Moreover, the spatial network structure of the nano-composites protects part of the functional groups on the polymer surface, which reduces the negative impacts of molecular chain shrinkage and hydrodynamic radius reduction caused by the neutralization of negative charges by cations in the solution, making the entire system capable of certain salt resistance properties.

3.3. Rheology

The slickwater-based fracturing fluid system will undergo multiple complex conditions when entering the target formation, such as high temperature and shear resistance. Besides, improving the salt resistance of slickwater-based fracturing fluid is helpful in making full use of the produced water with high salinity, reducing environmental pollution and saving economic costs (Seymour et al., 2018). To ensure that the MoS_2 nanosheet-modified DR-900 slickwater has sufficient temperature and shear resistance, salt resistance and excellent viscoelastic properties, a rheological test is required. This is to observe the potential effect of MoS_2 nanomaterial on the structure and rheological properties of the DR-900 slickwater system.

3.3.1. Temperature and shear resistance

At present, the temperature and shear resistance of the slickwater-based fracturing fluid is the most challenging problem in some high-temperature reservoirs. Fig. 9 shows the effect of temperature on the apparent viscosity of both DR-900 slickwater and the modified DR-900 slickwater. The temperature increased from 25 to 80 °C at a constant shear rate of 170 s^{-1}, and the apparent viscosity shows a decreasing trend with increasing temperature. However, at different test temperatures, the apparent viscosity of the modified DR-900 slickwater is much higher than the conventional DR-900 slickwater, indicating the introduction of MoS_2 nanosheets could improve the temperature resistance of the DR-900 slickwater system to a certain degree. Apart from this, the rheological test results at high temperatures also proved that the temperature and shear resistance of the nanosheet-modified DR-900 slickwater were significantly improved, as shown in Fig. 10. After shearing for 120 min under 90 °C and 170 s^{-1}, the final apparent viscosity of the nanosheet-modified DR-900 slickwater is about 20 mPa s higher than that of the conventional DR-900 slickwater, which could meet the requirements for most field operations. As analyzed above, the addition of MoS_2 nanosheets has a remarkable influence on the temperature and shear resistance of the DR-900 slickwater system. It is found that the microstructure formed by MoS_2 nanosheets and polymer drag reducer has better thermal stability. The MoS_2 nanosheets and polyacrylamide molecules formed a denser and more complex network structure through cross-linking. Therefore, the micro-network structure of the nanosheet-modified DR-900 slickwater system is less affected by temperature, and the temperature resistance of the system is obviously improved.

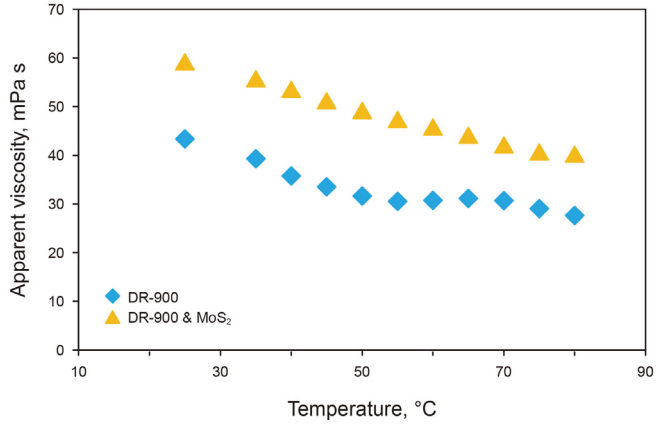

Fig. 9. Viscosity varies with temperature of two types of slickwater.

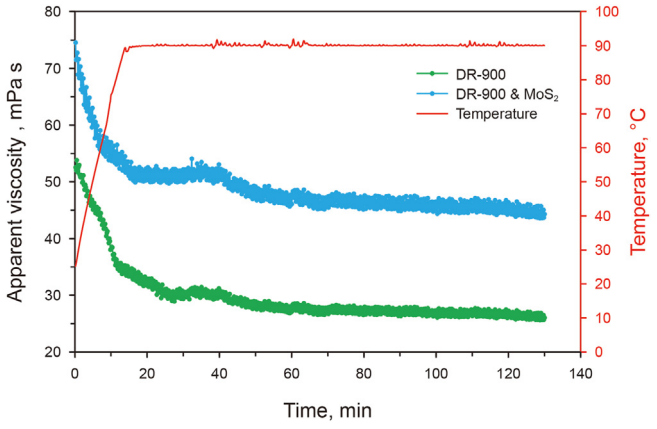

Fig. 10. Temperature and shear resistance of two types of slickwater.

3.3.2. Salt resistance

To investigate the effects of salinity on the rheological properties of the MoS_2 nanosheet-modified DR-900 slickwater fluid, NaCl, $MgCl_2$ and $CaCl_2$ were added to the freshwater to prepare a series of brines with different salinity. The apparent viscosity of the conventional DR-900 slickwater and the nanosheet-modified DR-900 slickwater in different types of salt solutions varies with the change of salinity, as shown in Fig. 11. The apparent viscosity of various slickwater systems at different brines gradually decreases with the increase of salinity, indicating that the salt ions seriously affect the overall apparent viscosity of the slickwater system. Taking the average value of the apparent viscosity of the same system under different salinity conditions, the average viscosity of the DR-900 slickwater-based fracturing fluid and the nanosheet-modified DR-900 slickwater-based fracturing fluid in different salt solutions can be obtained, as shown in Fig. 12. By comparison, it can be seen that under different salt solutions and salinity conditions, the apparent viscosity of the nanosheet-modified DR-900 slickwater system is significantly higher than that of the unmodified system. In addition, compared with Na^+, Ca^{2+} and Mg^{2+} have a greater negative impact on the apparent viscosity of slickwater; even the nanosheet-modified DR-900 slickwater also shows the same characteristic. These phenomena indicate that the negative effect of high-valent cations on the performance of polymer drag reducers is stronger than that of low-valent cations, which is consistent with the reports in related literature (Hazra et al., 2019, 2020; Nguyen et al., 2018). The addition of cations could effectively neutralize the negative charge in the polymer molecule chains, which brought about the shrinkage of molecule chains and the decrease of hydrodynamic radius. Compared with the monovalent cations, the shrinking effect of the chain dimension was more obvious when the multivalent cations were added. This is because the complex reaction occurred between high-valent cations and negatively charged groups on polymer surfaces, which not only shielded the electrostatic repulsion among anions but also effectively reduced charge densities around the macromolecule chain (Nguyen et al., 2018; Zhang et al., 2008). In addition, during the experiment, it was also found that the influence of Mg^{2+} on the viscosity of the slickwater is greater than that of Ca^{2+}, which is inconsistent with the conclusions in the existing literature. This may be related to the difference in ionic radius or threshold concentration of Ca^{2+} and Mg^{2+}, which needs to be further studied in the future.

3.3.3. Viscoelastic behavior

Viscoelasticity mainly focuses on the viscous modulus G'' and the elastic modulus G' of the tested fluid, which is one of the essential indicators to characterize the sand-carrying performance of fracturing fluid. It is generally assumed that the higher the elastic modulus of the fracturing fluid, the more favorable it is to carry proppant (Ba Geri et al., 2019; Bai et al., 2021; Biheri and Imqam, 2022).

To evaluate the viscoelastic characterizations of both DR-900 and nanosheet-modified DR-900 slickwater fracturing fluids, a small amplitude oscillatory shear test was carried out in the liquid solution's linear viscoelastic regime using the HAAKER RS6000 rheometer with a parallel-plate system at room temperature. Relaxation time is referred to as the inverse of the crossover point where the viscous modulus is equal to the elastic modulus. The lower the crossover frequency, the stronger the suspension ability of the proppant. Fig. 13 shows the G'' and G' of the two systems change with angular frequency. Both nanosheet-modified and unmodified DR-900 slickwater-based fracturing fluids show good elastic properties in the high relaxation time ranges. It can be found from the figure that the crossover value of the G'' and G' of the conventional DR-900 slickwater is 1.135 Pa, and the corresponding frequency is 0.0599 Hz; while the crossover value of the G'' and G' of nanosheet-modified DR-900 slickwater is 1.682 Pa, and the corresponding frequency is 0.0394 Hz. As we mentioned above, the fluid behaves as an elastic material at a frequency above the crossover point and as viscous material at a frequency below the crossover point. Since the nanosheet-modified DR-900 slickwater-based

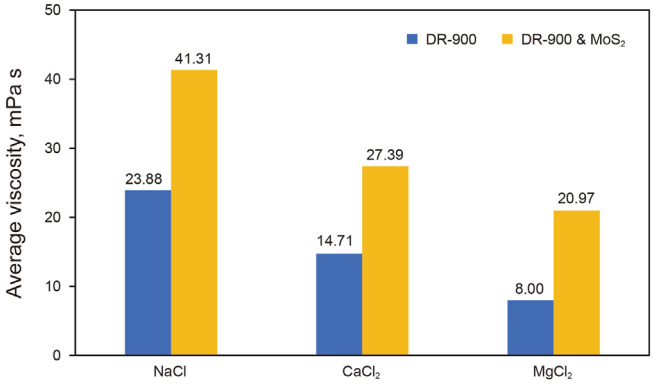

Fig. 12. Average viscosity of two types of slickwater under different salt types.

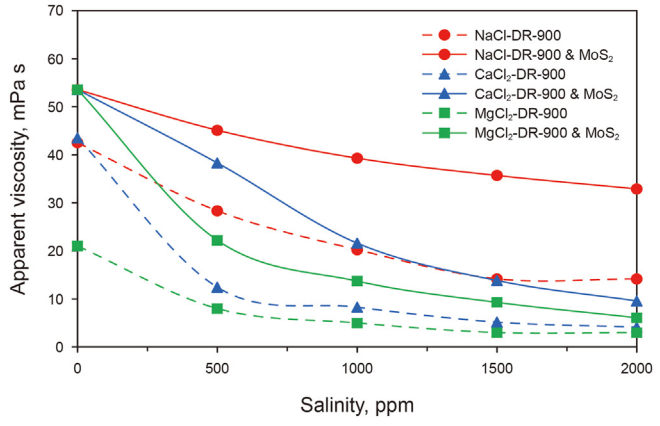

Fig. 11. Apparent viscosity changes with salinity and salt type of two types of slickwater.

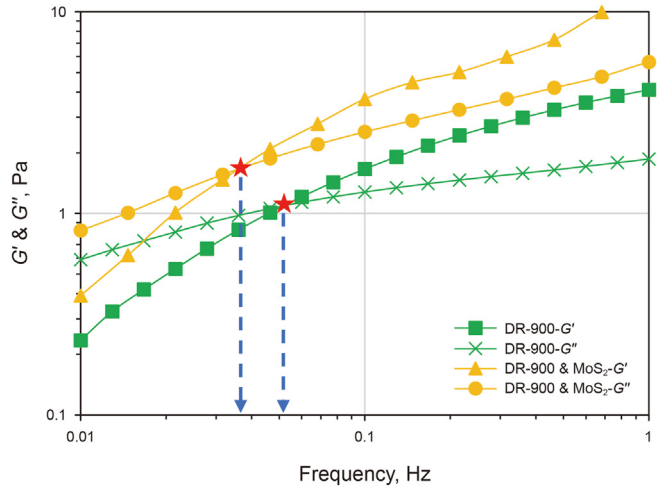

Fig. 13. Viscoelastic modulus curves and their crossovers of two types of slickwater.

fracturing fluid has a crossover frequency at 0.0394 Hz, it has a wider elastic regime, especially at low shear rate, compared to the conventional DR-900 slickwater which has the crossover frequency at 0.0599 Hz. Proppant suspension ability increases with reducing crossover frequency of the fluid. Hence, the introduction of MoS_2 sheets is beneficial for enhancing the sand-carrying capacity of the conventional DR-900 slickwater.

3.4. Nanosheet-modified DR-900 fracturing fluid performance

Excellent performance of fracturing fluid is a key factor affecting the effect of hydraulic fracturing and is directly related to the success or failure of fracturing stimulation. Compared with the guar gum fracturing fluid, the slickwater-based fracturing fluid has the characteristics of low drag, low viscosity, and low damage, which can meet the stimulation requirements of volumetric fracturing for large fluid and large displacement. However, the sand suspension performance of slickwater has always been criticized, although the excellent sand-carrying property is required to carry proppant into the deeper formation, support the hydraulic fractures and improve the fracture conductivity. In this section, drag reduction and sand suspension performance of the nanosheet-modified DR-900 slickwater system was evaluated successively.

3.4.1. Drag reduction

The drag reduction performance of the DR-900 fracturing fluid and the nanosheet-modified DR-900 slickwater system was evaluated with the loop drag test system in the room. The pipe diameter was 8 mm, while the tubing diameter used in most operation fields is 3.5 in. It is well-known that the flow velocity of the same displacement fluid in various pipe diameters is different, and the linear velocity can be used as an intermediate variable to match the experimental results in laboratory with the field practice. Linear velocity is defined as the fluid displacement divided by the cross-sectional area of the flow pipe, namely:

$$v = \frac{Q}{\rho \pi r^2} \tag{2}$$

where v is the linear velocity, m/s; Q is the displacement; ρ is the density of the fluid, kg/m^3; r is the pipe radius, m. Based on the equation, laboratory test results can be converted to the actual field displacement, as shown in Table 2.

Fig. 14 shows the drag reduction curves of the DR-900 slickwater system before and after modification at 20 and 80 °C, respectively. On the whole, the drag reduction efficiency of both slickwater-based fracturing fluids gradually increased with the increase of the test displacement. The increase is rapid in the low-velocity range of 1–7 m/s, and gradually tends to be stable in the high-velocity range of 7–13 m/s. The drag reduction performance of the nanosheet-modified slickwater was improved compared to the unmodified system, whether at 20 or 80 °C. At 20 °C, the maximum drag reduction rate increased from 72.9% to 76.3%, with an increased amplitude of 4.66%; at 80 °C, the maximum drag reduction rate increased from 65.4% to 67.4%, with an increased amplitude of 3.06%. Obviously, the addition of the MoS_2 nanosheets could enhance the drag reduction performance of the DR-900 slickwater-based fracturing fluid to a certain degree, especially in the high flow rate range. It is mainly because under high flow rates, the polymer molecular chain curled due to the electrostatic attraction will gradually expand, and the MoS_2 nanosheets will then act as nodes between polymer molecules. The nodes between the chains can protect the polymer molecules from shear fracture and maintain preferable drag reduction ability. Moreover, it is noteworthy that due to the power limit of the test equipment, the maximum lab test displacement is 2500 kg/h, and the corresponding field operational displacement is only 3.7 m^3/min. However, in the actual fracturing process, the pumping displacement always reaches 10 m^3/min or even higher, which is far beyond the range of laboratory test displacement. Drag reduction may be further improved at higher flow rates in the field, but overall, both slickwater systems were able to meet the operation demand for drag reduction efficiency greater than 60%.

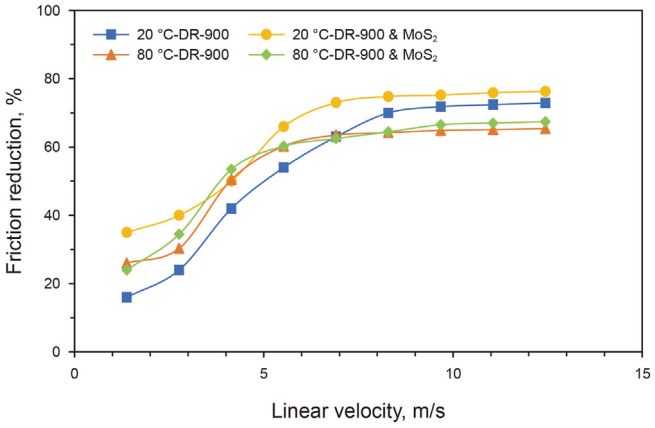

Fig. 14. Curves of drag reduction rate with linear velocity at different temperatures.

3.4.2. Sand suspension

The most convenient method to evaluate the sand suspension performance is to measure the settling velocity of various proppants in the fracturing fluid. Generally, the slower the settling velocity, the stronger the sand suspension capacity. In this work, the static sand settling is measured in the laboratory via specified graduated glasses. Both the conventional DR-900 slickwater and the nanosheet-modified DR-900 slickwater were used to evaluate sand settling with 20/40, 40/60, 60/80, 80/100 mesh sizes. Fig. 15

Table 2
Conversion of laboratory test displacement and field operational displacement.

Laboratory test displacement, kg/h	Linear velocity, m/s	Field operational displacement, m^3/min
250	1.38	0.37
500	2.76	0.74
750	4.14	1.11
1000	5.52	1.48
1250	6.90	1.85
1500	8.28	2.22
1750	9.66	2.59
2000	11.04	2.96
2250	12.42	3.33
2500	13.80	3.70

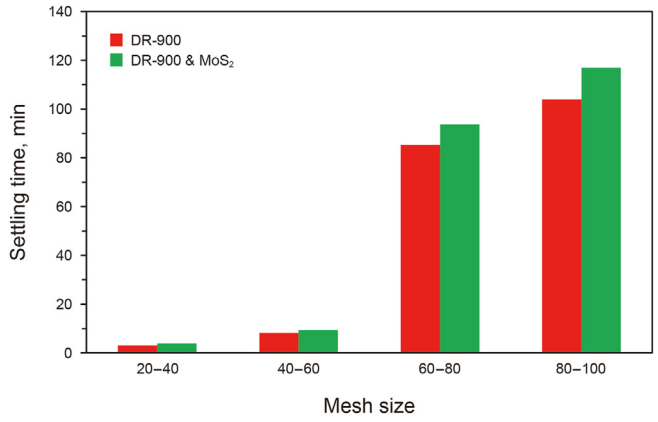

Fig. 15. Settling time of sand with different mesh in two types of slickwater.

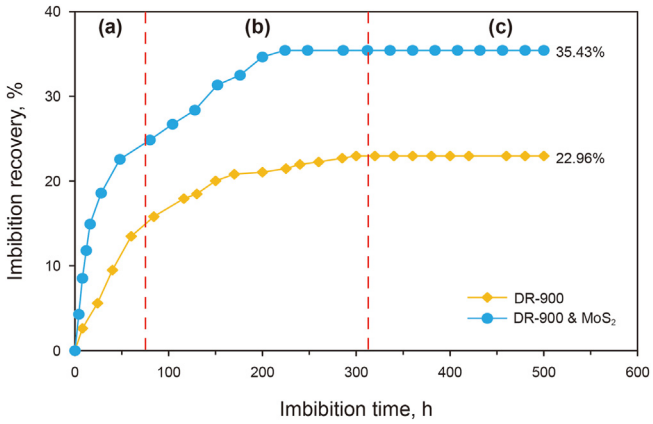

Fig. 16. Oil recovery versus time in spontaneous imbibition tests.

shows the settling time of sand with different mesh in the two types of slickwater-based fracturing fluids. It could be seen that the settling time of sand with different mesh sizes in nanosheet-modified DR-900 slickwater is increased compared with that in the conventional DR-900 slickwater. The settling time is the time consumed by the sand falling 140 mm height in the graduated cylinder, and the settling velocity of sand particles in each experiment can be further calculated, as shown in Table 3. The settling velocity of sand particles in the nanosheet-modified DR-900 slickwater system is slightly decreased, which could satisfy the requirements of the fracturing fluid and would not cause trouble such as sand plugging in the field application. Combining the viscoelasticity results of the two slickwater systems, the presence of MoS_2 nanosheets mainly increases the elastic modulus of the nanocomposites. This gives a good sand-carrying capacity during dynamic conditions (mixing and injection) with a small pressure drop during the injection because of its low viscosity at this condition. The increase in the density of the spatial network structure leads to an increase in the settling resistance of the proppant, showing a better suspension effect, so the overall sand-carrying performance of the nano-composites is significantly improved, in line with the conclusions in the existing literature (Biheri and Imqam, 2022; Gomaa et al., 2015).

3.5. Imbibition capacity

Fig. 16 shows the curve of imbibition oil recovery varies with time. As shown in the figure, the imbibition recovery of both DR-900 and nanosheet-modified DR-900 slickwater increased rapidly in the early stage and tended to be stable in the later stage. According to the variable shape of the curve, the imbibition process could be divided into (a) rapid imbibition stage, (b) slow imbibition stage, and (c) imbibition stable stage. For the DR-900 slickwater system, 0–60 h is the rapid imbibition stage, and about 13.48% of the oil was recovered; 50–300 h is the slow imbibition stage, and approximately 9.48% of the oil was recovered; after 300 h is the imbibition stable stage. For the nanosheet-modified DR-900 slickwater system, the rapid imbibition stage is 0–48 h, and about 22.57% of the oil was recovered; the slow imbibition stage is 48–245 h, approximately 12.86% of the oil was recovered, and the imbibition stable stage is after 245 h. The final imbibition recovery in conventional DR-900 and nanosheet-modified DR-900 slickwater gel-breaking fluid was 22.96% and 35.43%, respectively. The imbibition recovery increased by about 12.47% when the MoS_2 nanosheets were introduced, which indicates the nanosheet-modified DR-900 slickwater system has a higher oil imbibition efficiency. Further, imbibition recovery data were processed to obtain the relationship between imbibition rate and time, as shown in Fig. 17. It could be seen that the early imbibition rate of nanosheet-

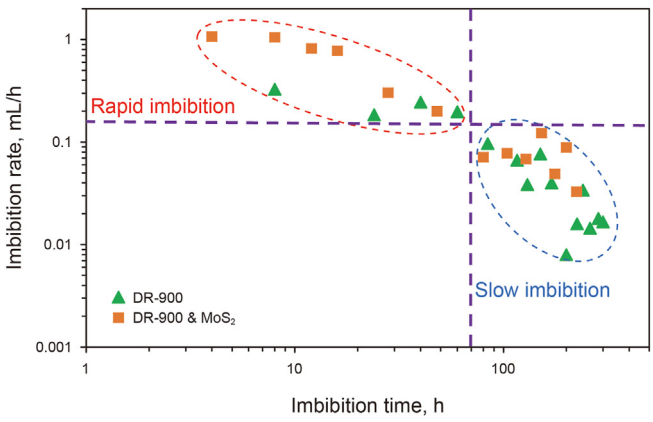

Fig. 17. Imbibition rate versus time in spontaneous imbibition tests.

Table 3
The settling velocity of sand with different mesh sizes in the two types of slickwater.

Fluid type	Mesh size	Settling distance, mm	Settling time, min	Settling velocity, mm/s
DR-900 slickwater	20/40	140	3.1	0.7527
	40/60	140	8.2	0.2846
	60/80	140	85.3	0.0273
	80/100	140	103.9	0.0224
Nanosheet-modified DR-900 slickwater	20/40	140	4.9	0.5983
	40/60	140	11.1	0.2482
	60/80	140	93.7	0.0249
	80/100	140	119.0	0.0199

modified DR-900 slickwater gel-breaking fluid was significantly higher than that of the unmodified DR-900 slickwater system. Higher rates and higher ultimate oil recovery make the nanosheet-modified slickwater a promising enhanced oil recovery agent in the unconventional reservoir hydraulic fracturing process.

3.6. Enhanced imbibition mechanism of MoS_2 nanosheets

The mechanisms of nanomaterials for enhanced imbibition and improved oil recovery have been greatly discussed in existing literature, such as wettability alteration, interfacial tension reduction, and mobility ration modification (Dai et al., 2017; Minakov et al., 2021; Nazari Moghaddam et al., 2015; Zhao et al., 2022). Actually, the interfacial tension between the nanosheet-modified slickwater gel-breaking liquid and kerosene was only 1.79 mN/m, which decreased significantly from 22.47 mN/m of the conventional DR900 slickwater. However, as the unique morphology, the "climbing film" theory would be preferable to reveal the major mechanism of MoS_2 nanosheets. To support this theory, a simple interfacial behavior experiment was conducted to determine the interfacial behavior of MoS_2 nanosheets under stimulated reservoir conditions. A typical procedure was as follows: an aqueous suspension of 0.1 wt% MoS_2 nanosheets was prepared and sonicated for 10 min. Ten milliliters of this suspension solution and 5 mL of kerosene were added to a 30-mL glass vial. Then the vial was gently shaken by hand for a few seconds, aiming to stimulate the local underground hydrodynamic power condition and prewetting the dry glass wall. By shaking, the dispersed MoS_2 nanosheets in the oil phase got an opportunity to accumulate at the oil/water interface, as shown in Fig. 18a. Most of the ultrasonic dispersion of MoS_2 nanosheets in the water phase aggregates at the oil-water interface and part of the oil phase after the shaking. As the number of nanosheets adsorbed on the interface increased, the interfacial tension was further decreased. After standing for 10 s, as shown in Fig. 18b, the climbing film was observed inside the blue dashed box above the vial. In the meanwhile, the volume of the oil phase in the yellow dashed box is slightly reduced, indicating part of the oil droplet was carried upward by the climbing film. As time went on, the color in the blue dashed box on the upper part of the vial gradually deepened, as shown in Fig. 18c. The change of color intensity is attributed to the increase of the interfacial concentration of MoS_2 nanosheets in the climbing film with increasing coalescence, and the concentration difference between the oil-water interface and vial wall gradually eases. At the same time, the volume of the oil phase in the yellow dashed box is further reduced. From the partially enlarged detail Fig. 18d, we can see there is an obvious climbing film above the oil phase surface in 20 s after shaking. The MoS_2 nanosheets are sparsely populated with the climbing film formed on the upper part of the oil phase, while the concentration of MoS_2 nanosheets in the oil phase is significantly higher than that of the vial wall. Movie S1 in Supplementary Material presents the whole process of MoS_2 nanosheets rapidly climbing the inner wall of the vial, and the concentration distribution of MoS_2 nanosheets tends to be balanced.

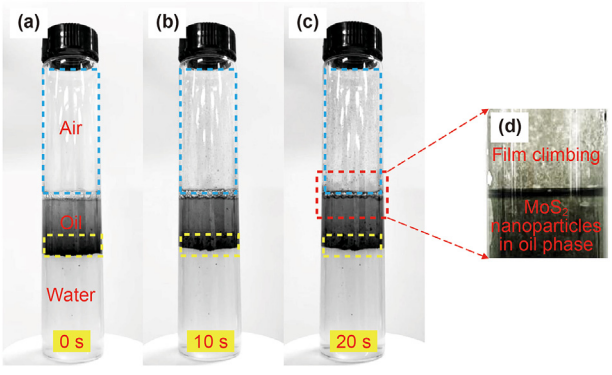

Fig. 18. Behavior of MoS_2 nanosheets forming a climbing film at different times: initial state (**a**); after standing for 10 s (**b**) and 20 s (**c**).

Supplementary video related to this article can be found at https://doi.org/10.1016/j.petsci.2022.12.008

The physical picture proposed to explain the above phenomenon is shown in Fig. 19. Since the vial wall is water-wet and the density of freshwater is greater than that of kerosene, the water underlies the oil phase and the MoS_2 nanosheets aggregate at the oil-water interface after gently shaking, which is presented in Fig. 19a. Interfacial tension between the oil phase and water decreased due to the accumulation of the MoS_2 nanosheets, and there is a concentration difference generated between the oil-water interface and the upper part of the vial. The climbing film was initially formed in Fig. 19b, because the locally raised nanosheet concentration induced spreading stress to push the oil-water interface up the vial surface. The essence of the spreading stress is the Marangoni effect caused by the gradient of interfacial tension, in which interfacially active MoS_2 nanosheets induce the spreading of the oil phase on the surface of the water solution (Cheng and Velankar, 2008; Luo et al., 2016). In three-phase regions (nanofluid, oil phase, and glass), the increased concentration of MoS_2 nanofluid inclined to form wedge-film structures and was forced to the oil-glass contact area (Dai et al., 2017; Gomaa et al., 2015). The ordering of this microstructure in the wedge-film region results in excess structural disjoining pressure in a film relative to that in the bulk solution, separating the two surfaces and limiting the nanofluid (Kondiparty et al., 2012). The disjoining pressure is related to the particle size and concentration of MoS_2 nanosheets. Generally speaking, smaller size and higher concentration tend to bring about higher disjoining pressure. When the structural disjoining pressure is greater than the adsorption force between the oil phase and glass surface, the vertex of the wedge film continues moving upward along the vial wall. Ultimately, under the action of the interfacial tension gradient, the continuous coalescence of the nanofluid droplet with the oil/water interface induces further climbing of the film, as shown in Fig. 19c.

During the spontaneous imbibition process of MoS_2 nanosheet-modified DR-900 slickwater gel-breaking fluid, the climbing film

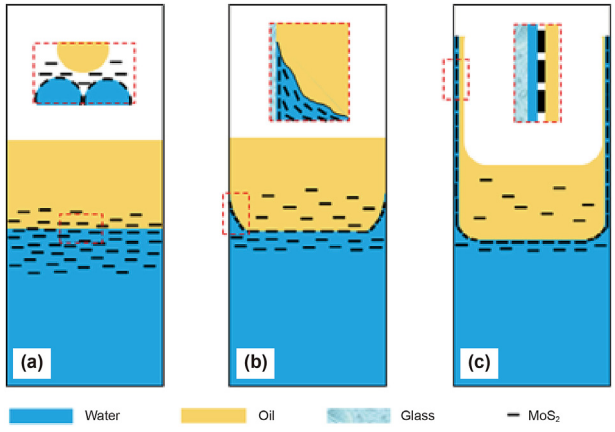

Fig. 19. Schematic illustration of interfacial film formation and climbing process. (**a**) MoS_2 nanosheets aggregate at the oil-water interface after shaking; (**b**) nanosheets start to form climbing film under wedge-shaped separation pressure; (**c**) nanosheets force the film to climb upwards.

was continuously formed due to the abundant hydrodynamic power. The presence of wedge film would act to detach oil from the porous media surface. Such extremely thin MoS_2 nanosheets possess high charge density and electrostatic repulsion, leading to the separation force at the wedge-film increase, thus leaving very little residual oil behind (Qing et al., 2022). In addition to these mechanisms, the nanosheets are expected to have a low chance of being trapped by the rock surface or plugging rock pores due to the self-accumulation of the oil-water interface, which may also contribute to high oil recovery efficiency (Alvarado et al., 2014; Yin et al., 2019). Based on the above work, it could be found that the presence of interfacial tension gradient and the formation of the climbing film may play an essential role in the spontaneous imbibition mechanism of the nanosheet-modified DR-900 slickwater system.

4. Conclusions

In this research, MoS_2 nanosheet was chemically synthesized by hydrothermal method and applied to formulate functional slickwater-based fracturing fluid. The microstructure characteristics and crystal type were analyzed by SEM, EDS, TEM, XPS, and Raman spectroscopy techniques. TGA and SEM methods were used to analyze the structure and morphology of the nanosheet-modified DR900 slickwater. The reaction mechanism of MoS_2 nanosheet with polymer was recognized, then the rheology, drag reduction, and sand suspension performance of the nanohybrid fracturing fluid were evaluated. Finally, spontaneous imbibition tests were carried out and the potential mechanism of MoS_2 nanosheet enhanced imbibition was clearly explained through an interfacial behavior experiment.

In the nano-composites, each MoS_2 nanosheet plays the role of cross-linking point, so as to make the spatial structure of the entire nano-composites more compact, and the interaction between MoS_2 nanosheets and polymer molecules is mainly through a covalent bond. Consequently, the nanosheet-modified DR-900 slickwater has better performance, reflected in thermal stability, salt resistance, viscoelasticity, drag reduction, and sand suspension ability. The nanosheet-modified slickwater has a higher apparent viscosity after shearing 120 min under 90 °C and 170 s^{-1}. The elastic characteristics of nanosheet-modified slickwater are more pronounced than that of the unmodified slickwater. Nanosheet-modified DR-900 slickwater achieves a drag reduction rate of 76.3% at 20 °C, with an increased amplitude of 4.66% compared with the conventional DR-900 system. Results of sand suspension experiments show that the sand settling time of proppants with different mesh in the nano-composites system was prolonged, and the sand settling velocity was decreased, indicating a dense network structure formed by the MoS_2 nanosheets is conducive to suspending the proppant. The spontaneous imbibition experiment shows that the final imbibition recovery rate of the gel-breaking fluid reaches 35.43%, and the early imbibition rate was significantly improved. The presence of an interfacial tension gradient and the formation of a climbing film may play an essential role in the spontaneous imbibition mechanism of the nanosheet-modified DR-900 slickwater.

In conclusion, MoS_2 nanosheets can obviously enhance the properties of slickwater-based fracturing fluids, and nanohybrids represent a new method for developing functional fracturing fluids.

Declaration of competing interest

The authors declare that they have no known competing financial interests or personal relationships that could have appeared to influence the work reported in this paper.

Acknowledgments

This research was financially supported by the National Natural Science Foundation of China (Grant Nos. 52004306 and 52174045), the Strategic Cooperation Technology Projects of CNPC and CUPB (Grant Nos. ZLZX2020-01 and ZLZX2020-02) and the National Science and Technology Major Projects of China (Grant Nos. 2016ZX05030005 and 2016ZX05051003).

References

Al-Muntasheri, G.A., Liang, F., Hull, K.L., 2017. Nanoparticle-enhanced hydraulic-fracturing fluids: a review. SPE Prod. Oper. 32 (2), 186–195. https://doi.org/10.2118/185161-PA.

Al-Sarkhi, A., 2010. Drag reduction with polymers in gas-liquid/liquid-liquid flows in pipes: a literature review. J. Nat. Gas Sci. Eng. 2 (1), 41–48. https://doi.org/10.1016/j.jngse.2010.01.001.

Alvarado, V., Bidhendi, M.M., Garcia-Olvera, G., Morin, B., Oakey, J.S., 2014. Interfacial visco-elasticity of crude oil-brine: an alternative EOR mechanism in smart waterflooding. In: SPE Improved Oil Recovery Symposium. https://doi.org/10.2118/169127-MS.

Ba Geri, M., Imqam, A., Bogdan, A., Shen, L., 2019. Investigate the rheological behavior of high viscosity friction reducer fracture fluid and its impact on proppant static settling velocity. In: SPE Oklahoma City Oil and Gas Symposium. https://doi.org/10.2118/195227-MS.

Bai, H., Zhou, F., Zhang, M., Gao, X., Xu, H., Yao, E., Li, Y., 2021. Optimization and friction reduction study of a new type of viscoelastic slickwater system. J. Mol. Liq. 344, 117876. https://doi.org/10.1016/j.molliq.2021.117876.

Barati, R., Liang, J.T., 2014. A review of fracturing fluid systems used for hydraulic fracturing of oil and gas wells. J. Appl. Polym. Sci. 131 (16). https://doi.org/10.1002/app.40735.

Bennion, D.B., 2002. An overview of formation damage mechanisms causing a reduction in the productivity and injectivity of oil and gas producing formations. J. Can. Pet. Technol. 41 (11). https://doi.org/10.2118/02-11-DAS.

Biheri, G., Imqam, A., 2022. Proppant transport using high-viscosity friction reducer fracture fluids at high-temperature environment. SPE J. 27 (1), 60–76. https://doi.org/10.2118/206750-PA.

Cao, B., Lu, X., Xie, K., Ding, H., Xiao, Z., Cao, W., Li, H., 2022. The pore-scale mechanisms of surfactant-assisted spontaneous and forced imbibition in water-wet tight oil reservoirs. J. Pet. Sci. Eng. 213, 110371. https://doi.org/10.1016/j.petrol.2022.110371.

Chen, H., Liu, H., Zhang, S., Feng, Y., 2020. Smart thermoviscosifying polymer for improving drag reduction in slick-water hydrofracking. Fuel 278, 118408. https://doi.org/10.1016/j.fuel.2020.118408.

Cheng, H.L., Velankar, S.S., 2008. Film climbing of particle-laden interfaces. Colloids Surf., A 315 (1–3), 275–284. https://doi.org/10.1016/j.colsurfa.2007.08.018.

Cheng, Y., 2012. Impact of water dynamics in fractures on the performance of hydraulically fractured wells in gas-shale reservoirs. J. Can. Pet. Technol. 51 (2), 143–151. https://doi.org/10.2118/127863-PA.

Cui, G., Tan, Y., Chen, T., Feng, X.T., Elsworth, D., Pan, Z., Wang, C., 2020. Multidomain two-phase flow model to study the impacts of hydraulic fracturing on shale gas production. Energy Fuels 34 (4), 4273–4288. https://doi.org/10.1021/acs.energyfuels.0c00062.

Dai, C., Wang, X., Li, Y., Lv, W., Zou, C., Gao, M., Zhao, M., 2017. Spontaneous imbibition investigation of self-dispersing silica nanofluids for enhanced oil recovery in low-permeability cores. Energy Fuels 31 (3), 2663–2668. https://doi.org/10.1021/acs.energyfuels.6b03244.

Edomwonyi-Otu, L.C., Chinaud, M., Angeli, P., 2015. Effect of drag reducing polymer on horizontal liquid–liquid flows. Exp. Therm. Fluid Sci. 64, 164–174. https://doi.org/10.1016/j.petrol.2006.11.002.

Geng, X., Sun, W., Wu, W., Chen, B., Al-Hilo, A., Benamara, M., Chen, T.P., 2016. Pure and stable metallic phase molybdenum disulfide nanosheets for hydrogen evolution reaction. Nat. Commun. 7 (1), 1–7. https://doi.org/10.1038/ncomms10672.

Gomaa, A.M., Gupta, D.V.S., Carman, P., 2015. Proppant transport? Viscosity is not all its cracked up to be. In: SPE Hydraulic Fracturing Technology Conference. https://doi.org/10.2118/SPE-173323-MS.

Habibpour, M., Clark, P.E., 2017. Drag reduction behavior of hydrolyzed polyacrylamide/xanthan gum mixed polymer solutions. Petrol. Sci. 14 (2), 412–423. https://doi.org/10.1007/s12182-017-0152-7.

Hazra, S., Madrid, V., Luzan, T., Van Domelen, M., Copeland, C., 2019. Correlating the performance of friction reducers with source water chemistry. In: SPE Oklahoma City Oil and Gas Symposium. https://doi.org/10.2118/195199-MS.

Hazra, S., Van Domelen, M., Cutrer, W., Peregoy, N., Okullo, P., Darlington, B., 2020. Performance of friction reducers in iron-rich environments. In: Unconventional Resources Technology Conference. https://doi.org/10.15530/urtec-2020-2487.

Ibrahim, A.F., Nasr-El-Din, H.A., Rabie, A., Lin, G., Zhou, J., Qu, Q., 2018. A new friction-reducing agent for slickwater-fracturing treatments. SPE Prod. Oper. 33 (3), 583–595. https://doi.org/10.2118/180245-PA.

Ismail, N., Alshami, A.S., Hussein, I.A., 2022. Synthesis and evaluation of a novel polyacrylamide functionalized nano-silica as a calcium carbonate inhibitor in

upstream applications. J. Pet. Sci. Eng. 209, 109864. https://doi.org/10.1016/j.petrol.2021.109864.
Keykhosravi, A., Vanani, M.B., Daryasafar, A., Aghayari, C., 2021. Comparative study of different enhanced oil recovery scenarios by silica nanoparticles: an approach to time-dependent wettability alteration in carbonates. J. Mol. Liq. 324, 115093. https://doi.org/10.1016/j.molliq.2020.115093.
Kondiparty, K., Nikolov, A.D., Wasan, D., Liu, K.L., 2012. Dynamic spreading of nanofluids on solids. Part I: experimental. Langmuir 28 (41), 14618–14623. https://doi.org/10.1038/nature01591.
Kot, E., Saini, R.K., Norman, L.R., Bismarck, A., 2012. Novel drag-reducing agents for fracturing treatments based on polyacrylamide containing weak labile links in the polymer backbone. SPE J. 17 (3), 924–930. https://doi.org/10.2118/141257-PA.
Krishnan, S., Abyat, Z., Chok, C., 2016. Characterization of boron-based nanomaterial enhanced additive in water-based drilling fluids: a study on lubricity, drag, ROP and fluid loss improvement. In: SPE/IADC Middle East Drilling Technology Conference and Exhibition. https://doi.org/10.2118/178240-MS.
Lafitte, V., Tustin, G., Drochon, B., Parris, M., 2012. Nanomaterials in fracturing applications. In: SPE International Oilfield Nanotechnology Conference and Exhibition. https://doi.org/10.2118/155533-MS.
Li, J., Huang, Q., Wang, G., Wang, E., 2022a. Influence of active water on gas sorption and pore structure of coal. Fuel 310, 122400. https://doi.org/10.1016/j.fuel.2021.122400.
Li, J., Huang, Q., Wang, G., Wang, E., Ju, S., Qin, C., 2022b. Experimental study of effect of slickwater fracturing on coal pore structure and methane adsorption. Energy 239, 122421. https://doi.org/10.1016/j.energy.2021.122421.
Li, M., Zhou, F., Yuan, L., Chen, L., Hu, X., Huang, G., Han, S., 2021. Numerical modeling of multiple fractures competition propagation in the heterogeneous layered formation. Energy Rep. 7, 3737–3749. https://doi.org/10.1016/j.egyr.2021.06.061.
Li, M., Zhou, F.J., Liu, J.J., Yuan, L.S., Huang, G.P., Wang, B., 2022. Quantitative investigation of multi-fracture morphology during TPDF through true tri-axial fracturing experiments and CT scanning. Petrol. Sci. 19 (4), 1700–1717. https://doi.org/10.1016/j.petsci.2022.03.017.
Li, W., Liu, J., Zeng, J., Tian, J., Li, L., Zhang, M., Jiang, J., 2019. A critical review of the application of nanomaterials in frac fluids: the state of the art and challenges. In: SPE Middle East Oil and Gas Show and Conference. https://doi.org/10.2118/195029-MS.
Li, W., Liu, J., Zeng, J., Leong, Y.K., Elsworth, D., Tian, J., Li, L., 2020. A fully coupled multidomain and multiphysics model for evaluation of shale gas extraction. Fuel 278, 118214. https://doi.org/10.1016/j.fuel.2020.118214.
Li, W., Liu, J., Zeng, J., Leong, Y.K., Elsworth, D., Tian, J., 2022. Water Liberating/Sealing effects on shale gas Extraction: a fully coupled multidomain and multiphysics model. Fuel 325, 124953. https://doi.org/10.1016/j.fuel.2022.124953.
Li, X., Pan, J., Shi, J., Chai, Y., Hu, S., Han, Q., Jing, D., 2022. Nanoparticle-induced drag reduction for polyacrylamide in turbulent flow with high Reynolds numbers. Chin. J. Chem. Eng. https://doi.org/10.1016/j.cjche.2022.07.015.
Li, Y., Zhou, F., Li, B., Cheng, T., Zhang, M., Wang, Q., Liang, T., 2022a. Optimization of fracturing fluid and retarded acid for stimulating tight naturally fractured bedrock reservoirs. ACS Omega. https://doi.org/10.1021/acsomega.2c01612.
Li, Y., Zhou, F., Wang, J., Li, B., Xu, H., Yao, E., Zhao, L., 2022b. Influence of nanoemulsion droplet size of removing water blocking damage in tight gas reservoir. At. Energ. 15 (14), 5283. https://doi.org/10.3390/en15145283.
Liu, H., Bai, H., Lv, B., Li, C., Liu, J., Huang, G., Zhou, F., 2022. Parameter optimization and field test of nano variable-viscosity slick water fracturing in Changqing shale reservoir. IOP Conf. Ser. Earth Environ. Sci. 984 (1), 012004. https://doi.org/10.1088/1755-1315/984/1/012004.
Liu, J., Wang, S., Wang, C., Zhao, F., Lei, S., Yi, H., Guo, J., 2020. Influence of nanomaterial morphology of guar-gum fracturing fluid, physical and mechanical properties. Carbohydr. Polym. 234, 115915. https://doi.org/10.1016/j.carbpol.2020.115915.
Liu, Z., Bai, B., Wang, Y., Qu, H., Xiao, Q., Zeng, S., 2021. Spontaneous imbibition characteristics of slickwater and its components in Longmaxi shale. J. Pet. Sci. Eng. 202, 108599. https://doi.org/10.1016/j.petrol.2021.108599.
Luo, D., Wang, F., Zhu, J., Cao, F., Liu, Y., Li, X., Ren, Z., 2016. Nanofluid of graphene-based amphiphilic Janus nanosheets for tertiary or enhanced oil recovery: high performance at low concentration. Proc. Natl. Acad. Sci. USA 113 (28), 7711–7716. https://doi.org/10.1073/pnas.1608135113.
Minakov, A.V., Pryazhnikov, M.I., Suleymana, Y.N., Meshkova, V.D., Guzei, D.V., 2021. Experimental study of nanoparticle size and material effect on the oil wettability characteristics of various rock types. J. Mol. Liq. 327, 114906. https://doi.org/10.1016/j.molliq.2020.114906.
Nazari Moghaddam, R., Bahramian, A., Fakhroueian, Z., Karimi, A., Arya, S., 2015. Comparative study of using nanoparticles for enhanced oil recovery: wettability alteration of carbonate rocks. Energy Fuels 29 (4), 2111–2119. https://doi.org/10.1021/ef5024719.
Nguyen, T.C., Romero, B., Vinson, E., Wiggins, H., 2018. Effect of salt on the performance of drag reducers in slickwater fracturing fluids. J. Pet. Sci. Eng. 163, 590–599. https://doi.org/10.1016/j.petrol.2018.01.006.
Nikolov, A., Kondiparty, K., Wasan, D., 2010. Nanoparticle self-structuring in a nanofluid film spreading on a solid surface. Langmuir 26 (11), 7665–7670. https://doi.org/10.1021/la100928t.
Qing, S., Chen, H., Han, L.J., Ye, Z., Liao, Y., Luo, Y., Yang, N., 2022. Effect of 2D alpha-zirconium phosphate nanosheets in interfacial tension reduction and wettability alteration: implications for enhanced oil recovery. SPE J. 27 (2), 986–998. https://doi.org/10.2118/208607-PA.
Rostami, P., Sharifi, M., Aminshahidy, B., Fahimpour, J., 2019. Enhanced oil recovery using silica nanoparticles in the presence of salts for wettability alteration. J. Dispersion Sci. Technol. https://doi.org/10.1080/01932691.2019.1583575.
Savjani, N., Lewis, E.A., Bissett, M.A., Brent, J.R., Dryfe, R.A., Haigh, S.J., O'Brien, P., 2016. Synthesis of lateral size-controlled monolayer 1H-MoS_2@oleylamine as supercapacitor electrodes. Chem. Mater. 28 (2), 657–664. https://doi.org/10.1021/acs.chemmater.5b04476.
Seymour, B., Friesen, D., Sanders, A., 2018. Enhancing friction reducer performance in high salt conditions. In: SPE/AAPG/SEG Unconventional Resources Technology Conference. https://doi.org/10.15530/URTEC-2018-2902709.
Shen, L., Khan, S., Heller, D., Fu, D., 2019. A cationic friction reducer fully compatible with produced water. In: SPE/AAPG/SEG Unconventional Resources Technology Conference. https://doi.org/10.15530/urtec-2019-129.
Song, Y.L., Gu, S.H., Song, Z.J., Zhang, Z.Y., Chang, X.Y., Guo, J., 2022. Effect of confinement on the three-phase equilibrium of water-oil-CO_2 mixtures in nanopores. Petrol. Sci. 19 (1), 203–210. https://doi.org/10.1016/j.petsci.2021.09.024.
Warholic, M.D., Massah, H., Hanratty, T.J., 1999. Influence of drag-reducing polymers on turbulence: effects of Reynolds number, concentration and mixing. Exp. Fluid 27 (5), 461–472. https://doi.org/10.1007/s003480050371.
Wei, C., Cheng, S., Wang, Y., Shi, W., Li, J., Zhang, J., Yu, H., 2021. Practical pressure-transient analysis solutions for a well intercepted by finite conductivity vertical fracture in naturally fractured reservoirs. J. Pet. Sci. Eng. 204, 108768. https://doi.org/10.1016/j.petrol.2021.108768.
Wei, C., Liu, Y., Deng, Y., Cheng, S., Hassanzadeh, H., 2022. Temperature transient analysis of naturally fractured geothermal reservoirs. SPE J. 1–23. https://doi.org/10.2118/205862-PA.
Xing, L., Ke, Y., Hu, X., Zhao, Y., Peng, F., Bai, C., Lin, Y., 2019. Preparation and properties of amphoteric polyacrylamide/modified montmorillonite nanocomposites and its drag reduction performance. Colloids Surf., A 574, 94–104. https://doi.org/10.1016/j.colsurfa.2019.04.078.
Xu, H., Zhou, F., Li, Y., Chen, Z., Yao, E., 2022. Development and evaluation of a novel high-density weighted fracturing fluid in ultra-deep reservoirs. IOP Conf. Ser. Earth Environ. Sci. 984 (1), 012015. https://doi:10.1088/1755-1315/984/1/012015.
Yao, E., Xu, H., Li, Y., Ren, X., Bai, H., Zhou, F., 2021. Reusing flowback and produced water with different salinity to prepare guar fracturing fluid. At. Energ. 15 (1), 153. https://doi.org/10.3390/en15010153.
Yekeen, N., Padmanabhan, E., Idris, A.K., Chauhan, P.S., 2019. Nanoparticles applications for hydraulic fracturing of unconventional reservoirs: a comprehensive review of recent advances and prospects. J. Pet. Sci. Eng. 178, 41–73. https://doi.org/10.1016/j.petrol.2019.02.067.
Yin, T., Yang, Z., Dong, Z., Lin, M., Zhang, J., 2019. Physicochemical properties and potential applications of silica-based amphiphilic Janus nanosheets for enhanced oil recovery. Fuel 237, 344–351. https://doi.org/10.1016/j.fuel.2018.10.028.
Yu, W.C., Jun, W., Baohang, H., 2015. Synthesis and application of green and clean nanometer composite drag reduction agent in shale gas development. J. Yangtze Univ. (Nat. Sci. Ed.) (8), 78–83. https://doi.org/10.16772/j.cnki.1673-1409.2015.08.019 (in Chinese).
Zhang, H., 2015. Research progress in the preparation and properties of nanometer-sized molybdenum disulfide. China Molybdenum Ind. 39 (3), 5–10. https://doi.org/10.13384/j.cnki.cmi.1006-2602.2015.03.002 (in Chinese).
Zhang, Q., Zhou, J.S., Zhai, Y.A., Liu, F.Q., Gao, G., 2008. Effect of salt solutions on chain structure of partially hydrolyzed polyacrylamide. J. Cent. South Univ. Technol. 15 (1), 80–83. https://doi.org/10.1007/s11771-008-0319-x.
Zhang, X., Xu, H., Wang, J., Ye, X., Lei, W., Xue, M., Li, C., 2016. Synthesis of ultrathin WS_2 nanosheets and their tribological properties as lubricant additives. Nanoscale Res. Lett. 11 (1), 1–9. https://doi.org/10.1186/s11671-016-1659-3.
Zhao, M., Cheng, Y., Wu, Y., Dai, C., Gao, M., Yan, R., Guo, X., 2022. Enhanced oil recovery mechanism by surfactant-silica nanoparticles imbibition in ultra-low permeability reservoirs. J. Mol. Liq. 348, 118010. https://doi.org/10.1016/j.molliq.2021.118010.